Eur Biophys J (1989) 17: 173–186

European Biophysics Journal

Hydration structure in natural DNA observed by thermal neutron scattering

H. Grimm [1]* and A. Rupprecht [2]

[1] Institut für Festkörperforschung, Kernforschungsanlage Jülich, P.O. Box 1913, D-5170 Jülich, Federal Republic of Germany
[2] Division of Physical Chemistry, Arrhenius Laboratory, University of Stockholm, S-10691 Stockholm, Sweden

Received February 2, 1989/Accepted in revised form August 3, 1989

Abstract. Films of highly oriented Na- and LiDNA showing the typical X-ray diffraction patterns for the A-, B-, and C-conformation have been investigated by elastic and quasielastic neutron scattering. Information concerning the question of the DNA–water interaction has been obtained by varying the parameters H_2O/D_2O contrast, humidity, and temperature. Main observations are: A coexistence of one- and three-dimensionally correlated DNA which shifts towards the one-dimensionally correlated C-conformation for high humidity; a coexistence of A-, B-, and C-conformation for NaDNA with a similar humidity dependence; a factor of two increase between the average degree of localization of water hydrogens compared with DNA hydrogens at 75% r.h. for NaDNA; a strong water contribution to layer peaks which are close to the susceptibility maximum of water; a strong temperature dependence of the axial repeat distance for C-DNA; broad quasielastic spectra around the inverse of this distance. The observations are interpreted in terms of a competition between finite three-dimensional correlation and an optimized spatial resonance of nearly one-dimensionally correlated DNA with the correlation of bulk water. The observations are compatible with the concept of water spine formation (Dickerson 1983). The interpretation emphasizes the dynamic character of this mechanism in the region of nearly one-dimensionally correlated DNA.

Key words: DNA hydration, neutron scattering

Introduction

X-ray diffraction by deoxyribonucleic acid (DNA) fibres has been the primary experimental method to unravel microscopic density–density correlations in this system. Since the observation of Franklin and Gosling (1953) – "the most highly ordered structure was that obtained when operating at about 75% r.h. (structure A)" – it has become progressively evident (Langridge et al. 1960; Marvin et al. 1961; Cooper and Hamilton 1966) that the four constituents, i.e. DNA-chains, counterions, water hull, and excess salt form a correlated system with a subtle interaction balance resulting in the stabilization of various conformations of DNA. Several reasons have led to attention being focussed mainly on DNA–DNA correlations. One reason is the mere ratio of atoms of the four constituents, i.e. per nucleotide one has typically 1 counterion ($1\,e^+$), 5–10 water molecules, and ≤ 0.4 molecules excess salt (e.g. NaCl, LiCl). Another reason is the degree of localization of these atoms which is reflected in the sharpness and intensity of the constructive interferences observed in reciprocal space. Compared to Bragg-reflections of ordinary crystals, DNA–DNA correlations give rise to rather weak signals due to the large thermal motion of the atoms. In addition to this thermal disorder, DNA-peaks are further weakened by static disorder, i.e. by the "random" sequence of base pairs along the chain and by randomness in the phase relation between neighboring DNA molecules. When trying to observe constructive DNA–water interference, one has to deal with even smaller and more diffuse signal since the localization of the water molecules is governed by the much weaker multipolar forces (compared to the covalent interactions within the chain which restrain the motion of the DNA-atoms). Thus, collecting microscopic information about the concerted interaction of the constituents of this complex system means the analysis of both the "Bragg-peaks" *and* the relatively smoothly varying diffuse scattering between them. Moreover, a significant part of the latter scattering is of inelastic nature because of the large thermal disorder which poses a further problem in the analysis of the diffuse scattering contributions.

In this situation one may either turn to similar systems which have a higher degree of translational

* To whom offprint requests should be sent

invariance and less thermal disorder or one changes to scattering methods which provide an informative discrimination between the various correlation contributions. The former concept has been successfully realized by Kopka et al. (1983). The results from oligonucleotide analysis have led to the conclusion (Dickerson 1983) that the formation of a water spine in the minor groove of B-DNA and the more economic hydration of the phosphate groups in A-DNA as compared to B-DNA (Saenger et al. 1986) are essential elements of the DNA–water stabilization.

We have followed the second approach by using thermal neutron scattering on natural DNA (calf-thymus). This method (e.g. Bacon 1975) provides a strong contrast on H_2O/D_2O-exchange and it can also discriminate between elastic and inelastic scattering contributions. Parts of this study have been published previously (Grimm et al. 1987, 1989). Neutron diffraction and H_2O/D_2O-contrast has also been used to determine the location of water around a synthetic DNA fiber in the D-conformation (Fuller et al. 1989).

Experimental

Materials

The difficulty of preparing oriented DNA-samples large enough for neutron scattering has been overcome by the development and perfection of the wet-spinning method (Rupprecht 1966). This method allows the controlled production of sufficient amounts of highly oriented, thin films (1 to 100 μm thickness) by winding up DNA fibres which are continuously stretched during precipitation into an aqueous alcohol solution. Films of 45 mm × 275 mm could be obtained in this way. They were prepared from calf-thymus DNA. The films were zig-zag folded into a square sample and – after humidification with H_2O or D_2O to the desired relative humidity – sealed into an aluminium cell with a free volume of $60 \times 60 \times 1$ mm^3. The illuminated sample volume was about $40 \times 40 \times 0.7$ mm^3. The first neutron scattering experiments on samples of this type were performed by Dahlborg and Rupprecht (1971) and Dahlborg et al. (1980).

We have continued this study by reinvestigating one of the samples used in these studies (No. 1, Li-DNA, C-conformation, ≃0.03 LiCl/nucleotide) and three new samples of higher crystallinity (No. 2, Na-DNA, A-conformation, ≃0.06 NaCl/nucleotide; No. 3, Li-DNA, B-conformation, ≃0.35 LiCl/nucleotide). Sample No. 4 is shown in Fig. 1. In this case, free standing films between two spring loaded grids were realized in order to allow for rapid in situ water exchange. Otherwise this sample is like No. 2. The various conformations of the DNA were verified by the typical X-ray diffraction patterns (Fig. 2) obtained from test pieces (75% r.h.). Generally, a qualitative

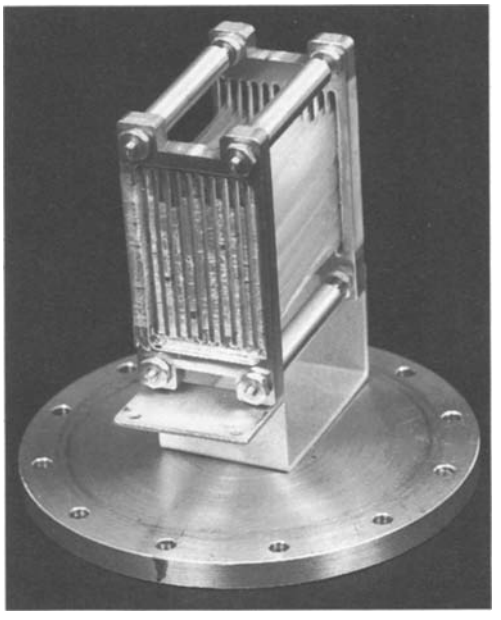

Fig. 1. Sample for in situ humidification. The total area is 35 mm · 28 mm · 21 films. The film thickness is about 50 μm. The DNA film is kept under slight tension by the four spring loaded cylinders which connect the two supporting grids

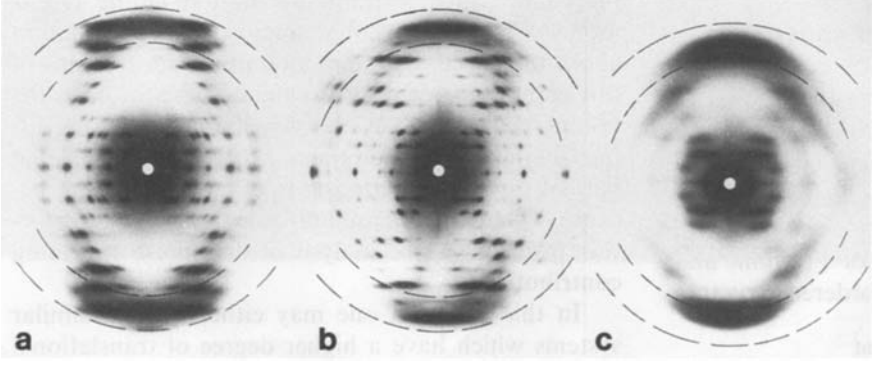

Fig. 2a–c. X-ray diffraction patterns as obtained from test pieces of the DNA films at 75% relative humidity. (**a**)–(**c**) are typical for the A, B, C-conformation. (**a**) corresponds to NaDNA (samples Nos. 2 and 4), (**b**) to LiDNA with high excess salt concentration (sample No. 3), and (**c**) to LiDNA with low excess salt concentration (sample No. 1). The *dashed circles* indicate the region of the first peak in the structure factor of bulk D_2O as obtained by neutron scattering (Fig. 3)

similarity is observed between X-ray and neutron diffraction patterns of DNA. This is due to the fact that the neutron scattering lengths of C, N, O, P, and D are all positive and similar (e.g. Bacon 1975). This positive scattering density normally outweighs the negative contribution from hydrogen ($\simeq 1$ H per 2 other atoms).

Method

The previous neutron scattering studies were partially impeded by flux and instrumental limits. Therefore, we have performed our measurements at reactors providing a higher neutron flux and on three-axis-spectrometers which allow for a flexible scanning of reciprocal- (**h**) and frequency- (ν) space. The wave vector **h** is represented in a cylindrical coordinate system by $\mathbf{h} = (\xi, \psi, \zeta)$. The components ζ and ξ denote the meridional and the equatorial direction with respect to the helix axis of DNA, respectively. Since we observed deviations of the diffraction from cylindrical symmetry it should be added that the component ξ was usually varied within the plane of the DNA films and all data refer to $\psi = 0$, if not stated otherwise.

Because of the mentioned results obtained by X-ray diffraction from oligonucleotides, we focussed our attention on the region of reciprocal space corresponding to the inverse distance of nucleotide planes. It coincides with the location of the first maximum in the structure factor of liquid water. Therefore, it is in this region where one might expect constructive interference due to those water molecules whose correlation to DNA is of intermediate strength, i.e. between that of liquid water and tight binding to DNA. The increase or decrease of this correlation is expected to be largely responsible for variations in the DNA–DNA correlation and/or conformational changes.

Most of the experiments presented in this report were done at the instrument SV4 at the FRJ2-reactor in Jülich. In addition, we have used the spectrometers H7 and H4M at the high flux reactor HFBR at the Brookhaven National Laboratory. In all cases, the incident and scattered neutrons were selected by pyrolytic-graphite crystals in conjunction with an average horizontal collimation of $\simeq 40'$. The initial energy of 3.55 THz allowed the suppression of higher-order scattered neutrons by means of an aligned pyrolytic-graphite filter. The full width at half maximum (FWHM $\equiv \delta$) of the energy or frequency resolution was $\delta\nu = 0.23$ THz for the elastic setting ($\nu = 0$) of the instruments. In the following, the term "elastic intensity" corresponds to this energy resolution.

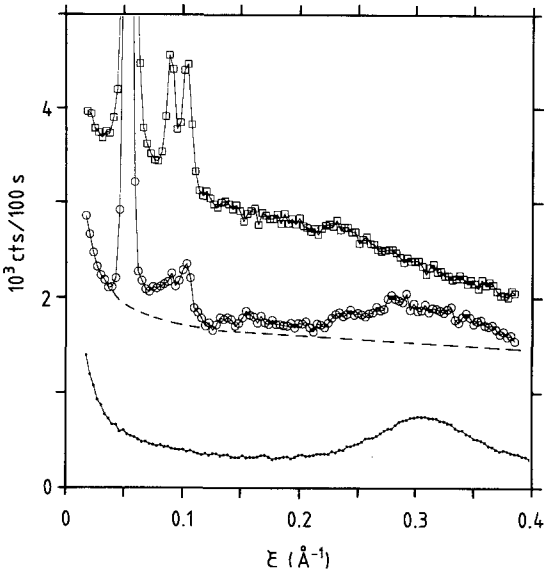

Fig. 3. Elastic scans perpendicular to helix direction for the NaDNA sample (No. 2) hydrated to 75% r.h. both with H_2O (*open squares*) and D_2O (*open circles*). The monotonously varying background is in both cases mainly due to the incoherent scattering from hydrogen. The *dashed line* indicates this and a small deuterium contribution for the case of hydration with D_2O. The scan for bulk D_2O (*full circles*) refers to the same experimental conditions (sample volume, spectrometer configuration)

Results

NaDNA – equatorial scans

Elastic scans perpendicular to the helix axis reveal the arrangement of the oriented DNA-molecules by means of the (hk0) reflections. Figure 3 shows scans of this type for NaDNA (sample No. 2) hydrated to 75% r.h. by both H_2O and D_2O. For the case of H_2O-hydration, three peaks are clearly distinguishable at $\xi = (0.052 \pm 0.001)$, (0.089 ± 0.001), and (0.102 ± 0.001) Å^{-1} on top of the monotonically decreasing incoherent background due to the hydrogen atoms. The peak positions follow closely the ratios $1 : \sqrt{3} : 2$ in accordance with an essentially hexagonal arrangement of the DNA-molecules. Their resulting effective diameter or the corresponding hexagonal lattice constant is $a = 2/(\sqrt{3}\, a^*) \simeq 22.2$ Å if a^* is based on the strong (1, 0, 0) reflection at $\xi \simeq 0.052$ Å^{-1} (Note, that the convention $\mathbf{a}\,\mathbf{a}^* = 1$ is used throughout this report). More precisely, A-DNA is described by a c-face centered monoclinic cell (Fuller et al. 1965).

Hydration with D_2O results essentially in three changes of this scan: (*i*) a distinct modification of intensities of the three DNA-reflections, (*ii*) a reduction of the background slope, and (*iii*) the appearence of the broad first maximum of the structure factor of D_2O at $\xi \simeq 0.31$ Å^{-1}. The latter fact becomes obvious if the scan is compared with the third curve (container filled

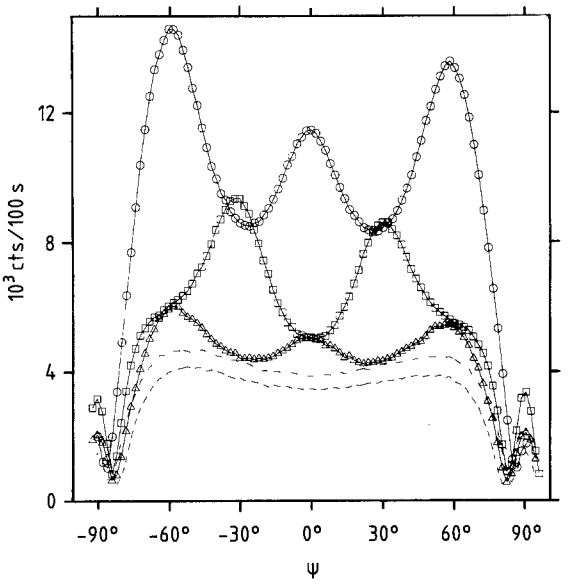

Fig. 4. Extended rocking curves for the equatorial reflections observed for H_2O-hydration (see Fig. 3). The momentum transfer was fixed to $\xi/\text{Å}^{-1}=0.052$ (*open circles*), 0.089 (*open squares*), and 0.102 (*open triangles*) and the sample rotated around the helix direction which was oriented perpendicular to the scattering plane. The symbol correspondence is (*open circles*)=(1, 0), (*open squares*)=(1, 1), (*open triangles*)=(2, 0) in hexagonal notation. The two *dashed curves* were obtained at the intermediate wave vectors $\xi/\text{Å}^{-1}=0.076$ (higher) and 0.127 (lower intensity). They represent the variation of the effective volume of the sample and the absorption due to incoherent scattering of hydrogen. The deep minima for each rocking curve around $\psi=\pm 90°$ denote the angles at which the incident or the scattered beam directions are oriented within the large area of the flat sample container

with D_2O). This means that some part of the water molecules are correlated in a similar way to liquid water.

Change (*i*) reflects the other part of the water which follows the symmetry of the array of DNA-molecules. The modifications of peak intensities correspond to changes of the average radial scattering density of this DNA-water molecule due to the replacement of H_2O by D_2O within the cylinder of about 11 Å radius around the helix axis.

It would be misleading to extract directly further conclusions about the radial water density from this limited data set of three intensity changes. Figure 4 shows rocking curves for these three reflections as obtained by rotating the sample around the helix axis at fixed ξ. The intensity variation shows that there is considerable double-orientation and confirms the essentially hexagonal arrangement of the DNA-polymers. The approximately equal intensities of the (110)- and the (200)-reflection observed in the radial scan at $\psi=0$ (Fig. 3) are seen to be an artifact which results from the "mosaic" of about 30° around the helix axis. Double orientation has been observed also with X-ray diffraction in wet-spun DNA films with Li- and Na-counterions (Wilkins and Arnott, personal communication with A. R.) and in a pulled NaDNA fibre (Franklin and Gosling 1953). It is interesting to note that the mean direction of **a*** is in the plane of the DNA-film. One might speculate whether the spinning procedure (Rupprecht 1966) causes this pinning. Probably, the boundary conditions enter during the drying procedure when the Teflon-coated cylinder is placed in a desiccator and the DNA fibres merge into an oriented DNA film. Double orientation is also observed for the LiDNA sample No. 3.

Change (*ii*), i.e. the change of background slope due to H_2O/D_2O exchange, contains information about the average degree of localization of the hydrogens of the water molecules and the hydrogens of DNA due to the large incoherent cross-section for protons. This incoherent background is indicated in Fig. 3 by the dashed line for the case of D_2O humidification and is evident for the case of H_2O humidification. We observe no significant difference of this background between equatorial and meridional scans. This might be due to our relatively coarse energy resolution of $\delta\nu=$ 0.23 THz. However, a similar isotropy has been observed in quasielastic spectra of incoherent neutron scattering (Schreiner et al. 1988) which probed the slower part of the motion of DNA–water with a frequency resolution of $\delta\nu=5$ GHz. This slower motion is found to correspond to diffusion within a sphere of 3–5 Å radius for high hydration levels (86% r.h.).

The isotropic incoherent background is also indicated in Fig. 5 by the straight dashed lines. The semi-logarithmic representation shows that it may be described by an effective Debye-Waller factor ($e^{-h^2B/2}$), at least on the time scale defined by our experimental resolution. The mean squared displacement $u^2=B/4\pi^2$ derived from the ξ- or ζ-dependence of the incoherent background is $u^2\simeq 0.046$ Å^2 for the case of D_2O-humidification and $u^2\simeq 0.076$ Å^2 for H_2O-humidification. On the basis of a fraction of 59% water-hydrogens for 75% r.h. or 8 moles water per mole nucleotide (Falk et al. 1962) a value of $u^2=(0.095\pm 0.010)$ Å^2 follows for the water hydrogens. The influence of a multiple scattering correction (Vineyard 1954) is estimated as being smaller than the generously estimated error. The fraction of water hydrogens is also compatible with the ratio of the background intensities extrapolated to $h=0$. Thus, the mean squared displacement of the average water hydrogen is about twice as large as that of the average DNA hydrogen which accounts for the background slope in the case of D_2O humidification. On the other hand, corresponding values reported for liquid water range from $u^2\simeq$ 0.3 Å^2 to $u^2\simeq 0.7$ Å^2 (Franks 1972). These large values may, however, only serve as a hint for the degree of hydrogen localization on the time scale of picoseconds

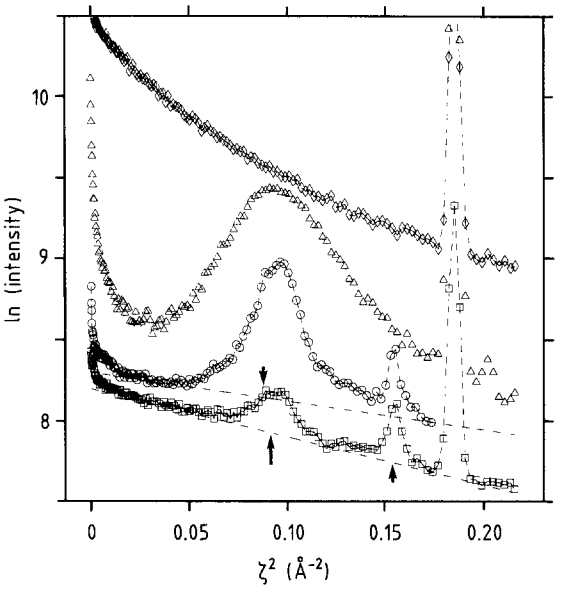

Fig. 5. Elastic scans along the helix direction ($\xi=0$) for sample No. 2 (NaDNA) hydrated to 75% r.h. both with D_2O (*open circles*) and H_2O (*open squares*). The *arrows* mark the expected peak locations due to the axial repeat distances for A-DNA (short, up), B-DNA (short, down), and C-DNA (long, up). The intensities are corrected for effective sample volume and absorption. The *dashed lines* represent the effective exponents of the Debye-Waller factor which describes the incoherent scattering. The *curves* obtained by filling the sample container with D_2O (*open triangles*) and H_2O (*open diamonds*) are added for comparison. The corrected intensities have been arbitrarily scaled in order to avoid intersection of the curves

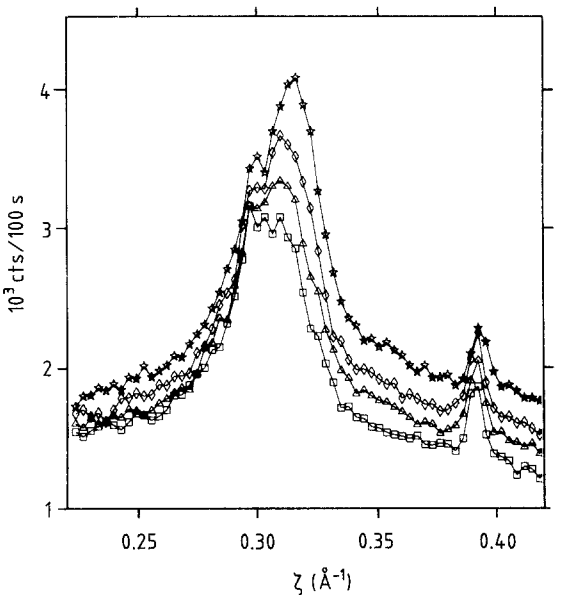

Fig. 6. Temperature variation of the meridional scan shown in Fig. 5 (symbol (*open circles*), D_2O-humidification). The symbols refer to sample temperatures of $T=320$ (*open squares*), 290 (*open triangles*), 260 (*open diamonds*), and 200 (*asterisks*) K

because of the artificial Debye-Waller type description. This is also evident from the curve for bulk H_2O in Fig. 5. The initial slope ($\zeta \to 0$) of this curve would correspond to $u^2 \simeq 0.4$ Å^2.

In summary, the equatorial test scans show that the oriented DNA-polymers of about 22 Å diameter follow essentially the expected hexagonal arrangement. It is found that this hexagonal lattice is only partly averaged around the helix axis and that otherwise **a*** has a mosaic distribution of about 30° FWHM with its mean direction in the plane of the DNA film. The scans also prove the expected sensitivity of the (hk0)-reflections on H_2O/D_2O-exchange and substantiate the intermediate degree of the average localization of the water molecules. Part of the water is correlated in a similar way to liquid water.

NaDNA – meridional scans

The effect of H_2O/D_2O contrast for scans along the helix direction is shown in Fig. 5. The representation of the data by logarithm of intensity versus ζ^2 is chosen in order to facilitate subtraction of the incoherent background. All data have been corrected for the weak ζ-dependence of effective volume and transmission of the samples. This correction factor increases with ζ in the displayed range by 10% and 14% for humidification to 75% r.h. with H_2O and D_2O, respectively.

Although the test of the sample (No. 2) by X-ray diffraction had shown the pattern being typical for the A-conformation (Fig. 2a), one recognizes in the meridional scans peaks due to the axial repeat distances p for all three conformations as indicated by the arrows. They correspond to the axial repeat distances $p_a=2.56$ Å, $p_b=3.38$ Å (Arnott and Hukins 1972), and $p_c=3.32$ Å (Marvin et al. 1961). For brevity, the peaks will be referred to as A-, B-, and C-peak below (the very small B-peak on the flank of the broad C-peak is more apparent in the linear presentation shown in Fig. 6). The strong peak at $\zeta^2=0.184$ Å^{-2} is the Debye-Scherrer line of Al (111) and results from the sample container. Its width corresponds to the instrumental resolution of $\delta\zeta=0.005$ Å^{-1} which decreases to $\delta\zeta=0.004$ Å^{-1} for $\zeta \simeq 1/p_b$. Resolution correction of the observed width of the A-peak results in a meridional correlation length $l_{\|} \simeq 45$ Å for the DNA with A-conformation. This peak is not much affected by the H_2O/D_2O exchange.

This is in contrast to the variation of the broad C-peak. Remarkable observations are: (*i*) the peak height more than doubles for humidification with D_2O (the peak/background ratio changes by a factor of about 4.8), and (*ii*) the peak shape changes with H_2O/D_2O exchange ("tail" for higher ζ-values). Further properties of the C-peak are, that its position is remarkably close to the position of the first maximum

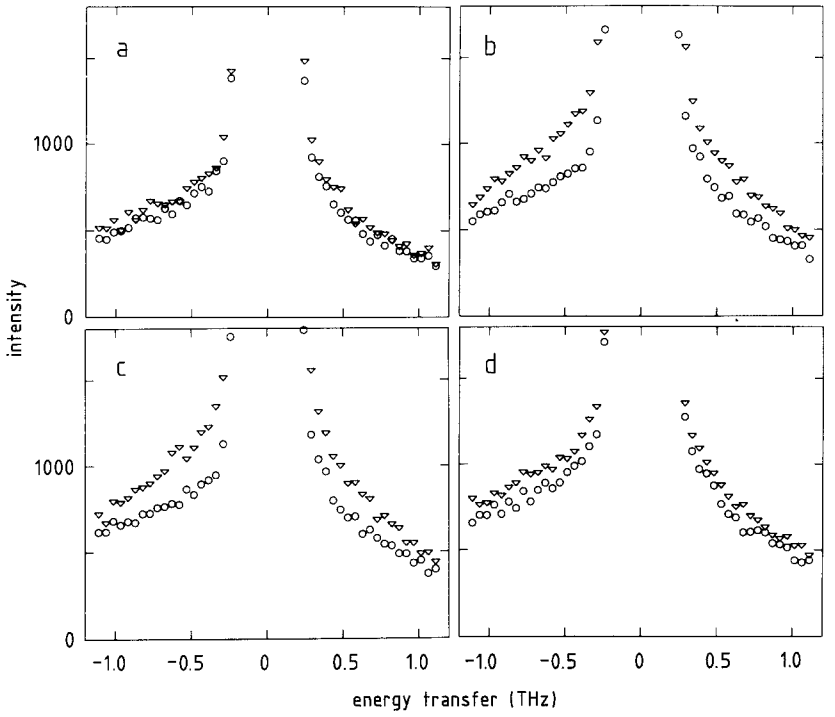

Fig. 7a–d. Intensity variation with energy transfer at fixed momentum transfer (**h**) oriented parallel (*open triangles*, $h=\zeta$) and perpendicular (*open circles*, $h=\xi$) to the helix axis. The correspondence for the wave vector is: $\boldsymbol{h}=\xi$, $\zeta=0.247$ Å^{-1} (**a**), 0.310 Å^{-1} (**b**), 0.323 Å^{-1} (**c**), and 0.374 Å^{-1} (**d**). The sample (No. 2, NaDNA) was humidified to 75% r.h. with D_2O

in the structure factor for liquid D_2O and would correspond to the somewhat smaller value of $p_c=3.27$ Å and that its width would correspond to a meridional correlation length of $l_{\|}\simeq 8$ Å, only.

We conclude from these observations that this peak contains a substantial contribution of intermediately correlated water whose correlation to DNA bridges that of the first hydration layer (Falk et al. 1962, 1963) and that of liquid water. This contribution will be referred to as "water peak" (WP) in the following.

Another means for distinguishing between WP and DNA-layer peaks is their different temperature dependence. This is shown in Fig. 6. The water structure corresponding to the WP contracts much more "rapidly" on temperature lowering than A- or B-DNA, as shown by the difference in the shift of the peak positions. Because of the larger shift of the WP, the B-DNA admixture becomes more apparent at lower temperatures.

NaDNA – low energy spectra at WP

One notices also that the WP region gains relatively more intensity on cooling than other regions of ζ (Fig. 6). As mentioned above, the measured intensity corresponds to a frequency resolution of $\delta\nu=$ 0.23 THz and the increase of intensity means that part of the inelastic spectra is shifted into this resolution "window". Thus, Fig. 6 suggests the existence of low-energy excitations associated with the WP. This has been verified by inelastic scans at fixed momentum transfers ζ which were compared to corresponding ones for ξ in order to discriminate the isotropic part of the spectra. The results for NaDNA are shown in Fig. 7. The difference between these scans represents excitations which involve mainly displacements **u** along the helix direction since the "visibility" is determined by the dot product **h u**, i.e. whether the motion gives rise to a phase shift in the scattered radiation.

Similar quasielastic difference spectra have been observed for the C-DNA sample (No. 1). A recently performed repetition of these measurements with smaller steps in the momentum transfer shows that the difference intensity clearly peaks at $\zeta\simeq 1/p_c$. The contributions from heavily damped compressional waves travelling along the helix direction become visible for $\zeta\neq 1/p_c$ just before the spectra vanish in the isotropic background. A report of these inelastic measurements will be published elsewhere. Underdamped compressional waves have been observed for B-DNA around $\zeta=1/p_b$ (Grimm et al. 1987). However, their damping is found to be more than three times larger than expected from the fluctuation δp_b. Overdamping occurs for changing the humidification from 75% to 84% r.h. (unpublished work).

We conclude from the WP contribution to the C-peak and the intermediate degree of localization of the water hydrogens that the difference spectra shown in Fig. 7 probably represent the hybridisation of relaxational motions of intermediately correlated water and oscillatory motions of the DNA bases (with or without tightly bonded water molecules) along the helix direction.

NaDNA – humidity variation

Information about the WP by means of humidity variation is ambiguous because of the simultaneous changes in the hydration structure and DNA conformation. However, compatibility with the interpretation based on contrast, temperature variation, and energy spectra of the WP can be tested.

If dried pieces of the DNA-films are exposed to an atmosphere of e.g. 75% r.h., their weight increases by a factor of $\simeq 1.45$ owing to water adsorption. More than 90% of this increase is completed within 24 h. We could make use of this time scale for in situ experiments by using a sample with free standing DNA-films (sample No. 4, Fig. 1).

To this end, a washing bottle with saturated D_2O-solution of $NaClO_3$ (corresponds to 75% r.h. at ambient temperature) was connected with the inlet and outlet of the sample container by rubber tubes. In this closed circuit, a forced convection of humidified air was maintained by means of a peristaltic pump. Valves allowed to switch this circuit to dried air (silicagel) or vacuum.

Three scans were measured alternatively during two humidification periods: (*i*) the meridional scan through the WP, (*ii*) a scan in meridional direction at $\xi = 0.111$ Å^{-1} which crosses the 6th-, 7th-, and 8th-layer lines of A-DNA at about their maximum intensity (see Fig. 2a), and (*iii*) a scan in equatorial direction at $\zeta = 0.283$ Å^{-1}, i.e. within the 8th layer. The results for the scans in meridional direction are shown in Fig. 8a and b. Three selected scans of type (*iii*) are compared in Fig. 9a and b to identical scans obtained from the other samples at fixed humidity levels.

The humidification history was as follows. Period I was started after 3 h of vacuum drying and lasted for about 17 h. The time interval between adjacent scans was 1.15 h. One scan took 20 min. Two things went wrong with the first attempt: (*i*) the drying period was obviously too short (WP had not vanished), and (*ii*) the chosen pump speed was too high. The latter caused an overshooting of the humidity level. The lack of equilibrium and of a calibrated humidity meter allowed us to only estimate the highest r.h.-level ($\simeq 90\%$). Period II was started after 23 h of drying with silicagel and lasted for about 18 h. Thereby, a saturated $NaNO_2$-solution (66% r.h.) was used and the pump speed was reduced. The time interval between adjacent scans was 2.6 h (apart from the "dry" scan). The two humidification periods are arranged in Fig. 8, according to increasing humidity and are separated by a constant level of intensity. The humidification period II (r.h. $\leq 66\%$) was repeated three times and good reproducibility of the intensity variations was observed. We conclude from these repetitions that the state of the sample at the end of period II was close to that for humidification to 66% r.h. at equilibrium conditions. The peak positions of the 6th-, 7th-, and 8th-layer lines correspond to a helical pitch of $P_a = (27.8 \pm 0.15)$ Å in this region and at the beginning of period I. Further information about the approximate humidity scale results from the comparison with the similar sample (No. 2) being equilibrated to 75% r.h. D_2O. Best correspondence with the value of $P_a = (28.1 \pm 0.15)$ Å resulting from the 11th-layer line (Fig. 5) was observed

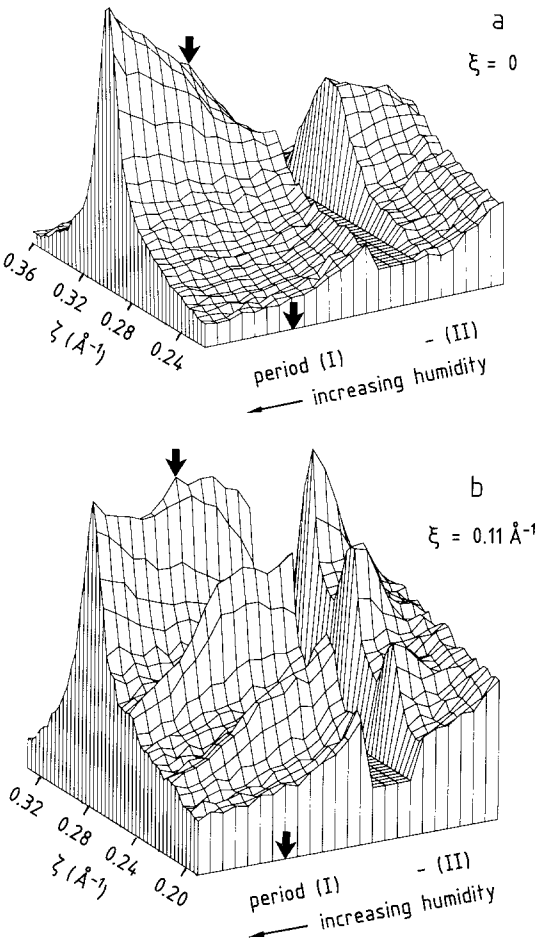

Fig. 8a and b. Humidity variation of two elastic scans in meridional direction for NaDNA (sample No. 4). (**a**) and (**b**) correspond to $\xi = 0$ and $\xi = 0.11$ Å^{-1}, respectively. The humidification history is described in the text. The *arrows* mark the state of humidification at which closest similarity to the equilibrated sample No. 2 (75% r.h., D_2O) was observed

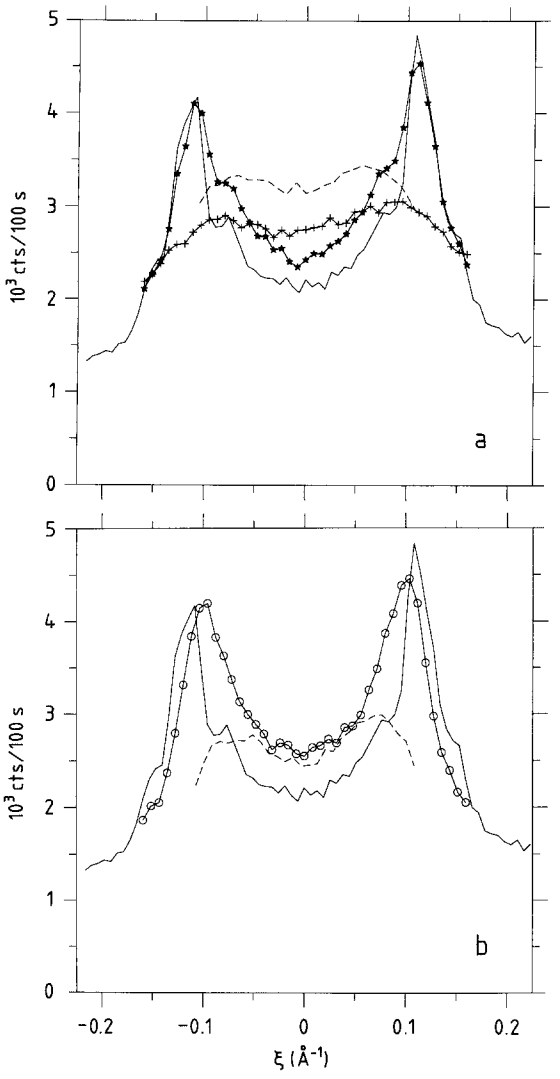

Fig. 9a and b. Comparison of intensity profiles at $\zeta = 0.283$ Å^{-1} (8th layer of A-DNA) at selected states of the in situ humidification of sample No. 4 (*symbols* plus *lines*) with corresponding scans obtained for the other samples being equilibriated to 75% r.h. with D_2O (*lines* only). All *curves* are independently scaled by the incoherent background from hydrogen in order to correct for differences in sample volume and neutron flux. (**a**) dried status at the start of period II (+), status marked by *arrow* in Fig. 8 (*asterisks*). The *solid line* corresponds to the NaDNA sample (No. 2) and the *dashed line* to the LiDNA sample (No. 1, low excess salt concentration). (**b**) status at the end of period I (*open circles*). The *solid line* is the same as for (**a**). The *dashed line* corresponds to the LiDNA sample (No. 3, high excess salt concentration)

for about the middle of period I (marked by arrow in Fig. 8). The close correspondence in the intensity profile within the 8th layer is shown in Fig. 9a. The intensity at $\xi = 0$ was lowest at this state of humidification and did not reach the level for the equilibriated sample.

The monotonic rise of the WP (Fig. 8a) with humidity can be considered as further hint for its identification. As expected, the 6th- and 7th-layer peaks (Fig. 8b) pass through a maximum of intensity owing to the stabilization of the A-conformation at the optimum humidity of about 75%. The behaviour of the 8th-layer peak is puzzling at first sight. In the region of over-humidification (end of period I), it gained intensity again and shifted thereby from $\zeta \simeq 0.285$ Å^{-1} to $\zeta \simeq 0.280$ Å^{-1}. This means a shift from 28.1 Å to 28.5 Å in terms of the helical pitch P_a. This difference in the humidity dependence may be interpreted as reflecting the transition to the B-conformation at about 90% r.h. (Cooper and Hamilton 1966) and/or a growing contribution of correlated water to the 8th-layer peak. Therefore, the intensity profile within the 8th layer for the end of period I is compared to corresponding scans obtained for samples No. 2 and No. 3 in the A- and B-conformation in Fig. 9b. The comparison with A-DNA shows that the 8th-layer peak has somewhat shifted to a lower value of ξ, however, the intensity profile is still markedly different from that for B-DNA. An interpretation of these differences in terms of changes in the orientation and position of the bases will be discussed below.

The alternative suggestion of a growing water contribution to the 8th-layer peak – similar to that of the WP to the C-peak – is supported by the vicinity in the modulus of the wave vector for both peaks and the ridge of intensity connecting them as shown in the next section. This would be consistent with the expectation that the intermediately correlated water is represented by an intensity pattern in **h**-space which is intermediate between that for liquid water and that for DNA, e.g. a highly textured ring. The possible region for such a ring-like pattern is indicated in Fig. 2 by dashed circles. They represent the FWHM contour of the peak for liquid D_2O shown in Fig. 3.

NaDNA, LiDNA – intensity pattern in the WP region

As suggested by the X-ray diffraction pattern (Fig. 2a), the WP actually represents a cut through a disk-like intensity distribution. Evidence for this shape has been found by mapping the elastic scattering intensity in the ζ, ξ-region of the WP. The resulting relief map of scattering intensity for NaDNA (Fig. 10a) includes DNA-peaks of the 7th, 8th, and 9th layer at $\zeta = 0.249$, 0.285, and 0.320 Å^{-1}, respectively. One notes that in the neutron relief the disk is more clearly located *between* the 8th and 9th layer whereas it is closer to the 8th layer for X-ray diffraction (Fig. 2a). We interpret this difference as being due to the fact that neutrons "see" both the O,O- and O,D-interference for water with about equal strength since both atoms have similar scattering lengths. In addition to the disk-like intensity distribution, one notes a ridge of intensity connecting the

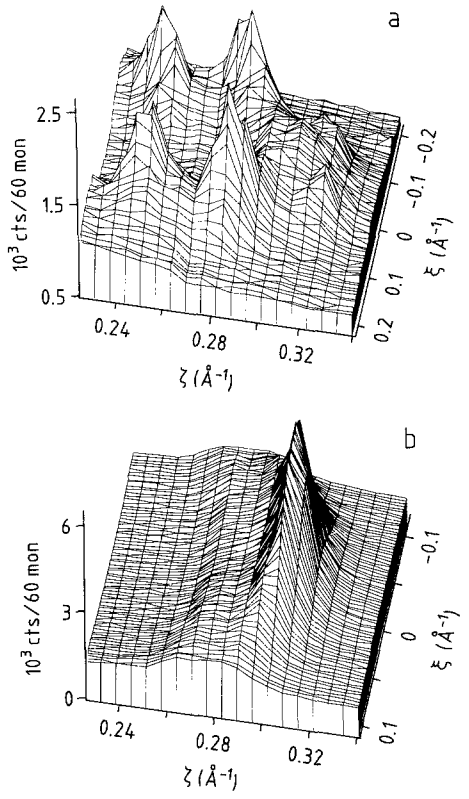

Fig. 10a and b. Relief maps of elastic intensity in the ξ, ζ-region containing the WP for (**a**) the NaDNA sample No. 2 and (**b**) the LiDNA sample No. 1. Both samples were equilibrated to 75% r.h. with D_2O. Note the factor of 2 in the mapped range of ξ between (**a**) and (**b**)

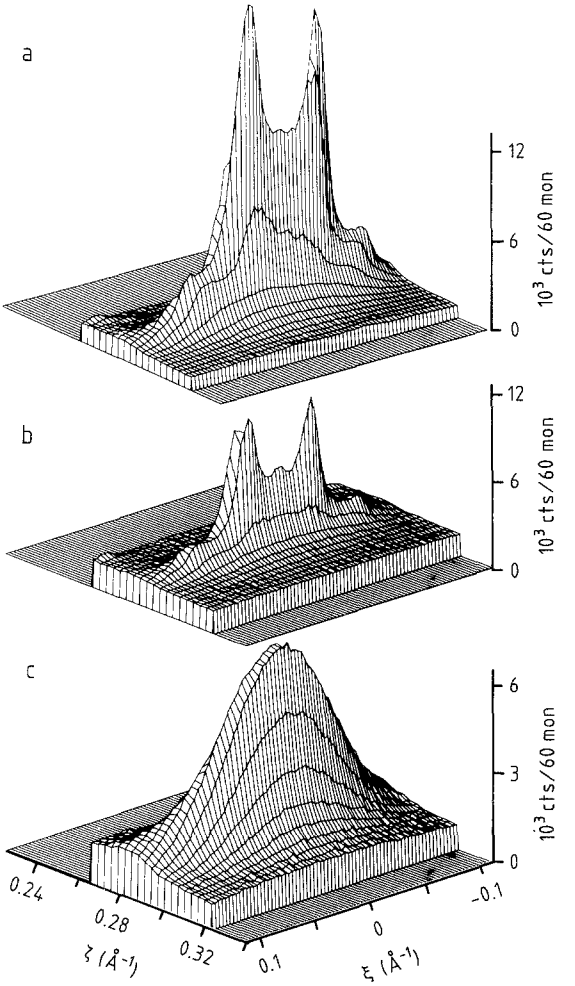

Fig. 11a–c. Same as Fig. 10 but for LiDNA (sample No. 3, high excess salt content). (**a**) corresponds to 75% r.h. D_2O-humidification, (**b**) to 75% r.h. H_2O, and (**c**) to 84% r.h. D_2O. Note the change of the intensity scale for case (**c**). The ξ, ζ-region indicated for zero intensity corresponds to that shown in Fig. 10b

8th-layer peak and the WP. The obvious incommensurability between the position of the WP and the helical pitch of A-DNA means that the WP cannot be part of the diffraction pattern for the A-conformation.

Figure 10b shows a similar relief map as Fig. 10a but with half the ξ-extension for the C-conformation with its non-integral number of base pairs per helical pitch (sample No. 1, LiDNA, low excess salt concentration). By this map it becomes clear that the WP of this previously studied (Dahlborg et al. 1980) sample contains both a disk-like part and a highly textured ring-like contribution. The latter contribution may be indicative of less correlated water which tends to follow the ring-like pattern of liquid D_2O. The position of the disk corresponds to an axial repeat distance of $p_c = (3.31 \pm 0.04)$ Å and its thickness results in a meridional correlation length of (18 ± 2) Å. The replacement of D_2O by H_2O results in a reduction of the disk intensity by a factor of about 2. This magnitude of the contrast is similar to that observed for NaDNA (sample No. 2).

The intensity patterns obtained for the other LiDNA sample (No. 3, LiDNA, high excess salt concentration) are shown in Fig. 11. In this case, the X-ray diffraction pattern at 75% r.h. (Fig. 2b) corresponds to the B-conformation with the integral value of 10 base pairs per helical pitch and the relief maps represent the intensity in the 10th layer of B-DNA. Three humidifications are compared. Figure 11a and b shows the result for humidification to the optimum humidity for the B-conformation (75%) with D_2O and H_2O, respectively. Additional peaks on top of the disk-like scattering are recognizable which signal the appearance of interhelical correlation in contrast to C-DNA. This correlation is however of finite range since for complete three-dimensional order the disk-like scattering would vanish. Both the mosaic of the helix axis η (FWHM) and the lateral correlation length contribute to the width of these peaks in the equatorial direction. Because of this mixed influence, any value for the lateral correlation between next neighbour dis-

tance and infinity may be derived from this observation for $1.9° \leq \eta \leq 3.3°$. As a second qualitative difference to C-DNA one observes that the ring-like contribution has practically vanished. The intensity difference between Fig. 11 a and b shows again the factor of about 2 for the disk intensity on D_2O/H_2O-exchange. The position of the disk corresponds to an axial repeat distance of $p_b = (3.38 \pm 0.02)$ Å and its thickness results in a meridional correlation length of (55 ± 5) Å. Thus, in the sequence WP, C-, and B-DNA, one observes a monotonous increase in the axial repeat distance and the meridional correlation length.

A reversal of this tendency, i.e. a change towards the intensity pattern for C-DNA, occurs for increasing the humidity of sample No. 3 above the optimum value of 75%. This is demonstrated by Fig. 11 c. The increase of the humidity to 84% causes the disappearance of the lateral correlation, a somewhat lower axial repeat distance of $p_b = 3.36$ Å, a significantly lower meridional correlation length of $\simeq 27$ Å, and again the indication of the ring-like intensity contribution. A decrease in the interhelical correlation is also observed for a reduction of the humidity to 66% as shown by the comparison of the intensity profiles at $\zeta = 1/(3.38$ Å) in Fig. 12. The intensity of the disk-like contribution ($\simeq$proportional to the meridional correlation length) is seen to pass through a maximum for humidification to 75%. This growth and decay of the three-dimensional correlation between 66% and 84% r.h. is in qualitative agreement with the change of Raman spectra obtained from a similar sample (Demarco et al. 1985). If interpreted as interhelical mode with the lowest restoring force, the transition from the spectral shape "overdamped" (66% r.h.) to "underdamped" (75% r.h.) and again to "overdamped" (86% r.h.) reflects the lifting of the degeneracy of the one-dimensional compressional waves which become phase related for three-dimensional correlation.

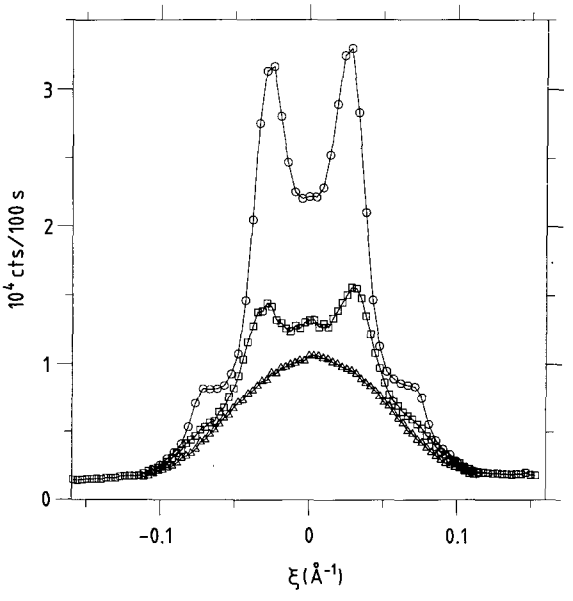

Fig. 12. B-DNA (sample No. 3): Comparison of the intensity profiles in the 10th layer ($\zeta = 0.296$ Å^{-1}) for three levels of D_2O hydration, 66% (*open triangles*), 75% (*open circles*), and 84% (*open squares*)

Discussion

Geometric aspect of DNA–water interaction

A key to a better understanding of the geometric aspect of the *mutual* DNA-water stabilization seems to be an argument given by Axe (1980) in the context of a model compound for quasi-one-dimensional systems. We repeat it below since the observed systematic trends in periodicity and correlation for A-, B-, and C-DNA indicate its relevance for the intermediate humidity range between already occupied primary hydration sites and the onset of the excessive swelling (Edwards et al. 1986).

Let $\varrho_0(\mathbf{r})$ represent the DNA density together with the strongly bonded first hydration layer and $\varrho(\mathbf{r})$ the density of the intermediately correlated water. Assume further a potential $\Phi_0(\mathbf{r})$ being associated with $\varrho_0(\mathbf{r})$ (i.e. same symmetry) which acts on $\varrho(\mathbf{r})$. If $\varrho_0(\mathbf{r})$ and $\varrho(\mathbf{r})$ would be perfectly periodic with reciprocal lattice vectors $\mathbf{G}_0$ and $\mathbf{G}$, the mutual interaction energy is

$$V = \int \Phi_0(\mathbf{r})\, \varrho(\mathbf{r})\, d\mathbf{r} = \sum_{\mathbf{G}_0, \mathbf{G}} \hat{\Phi}_0(\mathbf{G}_0)\, \hat{\varrho}(-\mathbf{G})\, \delta(\mathbf{G}_0 - \mathbf{G}), \quad (1)$$

where $\hat{\Phi}_0(\mathbf{G}_0)$, $\hat{\varrho}(\mathbf{G})$ denote the Fourier transform of $\Phi_0(\mathbf{r})$, $\varrho(\mathbf{r})$, respectively. The δ-function implies that both structures interact by virtue of common reciprocal lattice vectors. If the structures are incommensurate, they may interact via their spatially averaged properties ($\mathbf{G}_0 = \mathbf{G} = \mathbf{0}$), only. An example of such a property would be the macroscopic dielectric constant or susceptibility of water. However, the DNA–water system may gain additional interaction energy if both components $\varrho_0(\mathbf{r})$ and $\varrho(\mathbf{r})$ develop modulations with common periodicities or, equivalently, common wave vectors. Thus, one might expect, that a variation in the overlap of the diffraction contributions from DNA and water signals a variation in their strength of interaction. This means – in the language of linear response – that both components try to achieve spatial resonance since, according to the fluctuation-dissipation theorem, the diffraction pattern represents (besides atomic form factors or nuclear scattering lengths) the imaginary part of the generalized frequency and wave vector dependent susceptibility.

The susceptibility of liquid water (integrated over the frequency resolution of $\delta \nu = 0.23$ THz) is approxi-

mately given by the broad peak at $h_w \simeq 0.31$ Å^{-1} observed for D_2O (Fig. 3) since O and D have similar scattering lengths. One criterion for the optimization of the DNA-helix should then be whether large diffraction peaks (both elastic and quasi-elastic) are found in the neighborhood of the ring with radius h_w. These are the 10th-layer peak for the B-conformation and the off-meridional 8th-layer peaks for the A-conformation. The axial repeat distance for C-DNA is $\simeq 2\%$ smaller than for B-DNA and has a larger fluctuation. This shifts the broader C-peak (and WP) closer to h_w and provides a somewhat better overlap with the liquid water susceptibility. In addition, the fluctuation of the axial repeat distance p_c contains an appreciable dynamic component as shown by the strong temperature dependence of the peak position and the associated quasi-elastic spectra. From this point of view, the C-conformation is best suited for the interaction with water. This is of course only *one* principle in competition with others, e.g. the optimization of the interhelical interaction. In this case, the achievement of an integer number of base pairs per turn is important for the energy gain by the interhelical lock-in transition.

In the following, the neutron molecular formfactors of A- and B-DNA are considered with special emphasis on the region of h_w. The relation of the molecular formfactor and configuration of DNA to the X-ray diffraction patterns has been extensively discussed (Langridge et al. 1960; Marvin et al. 1961; Fuller et al. 1965). In the present context we seek a highly simplified translation of the information in **h**-space into real space in order to facilitate the discussion of our limited experimental data in **h**-space.

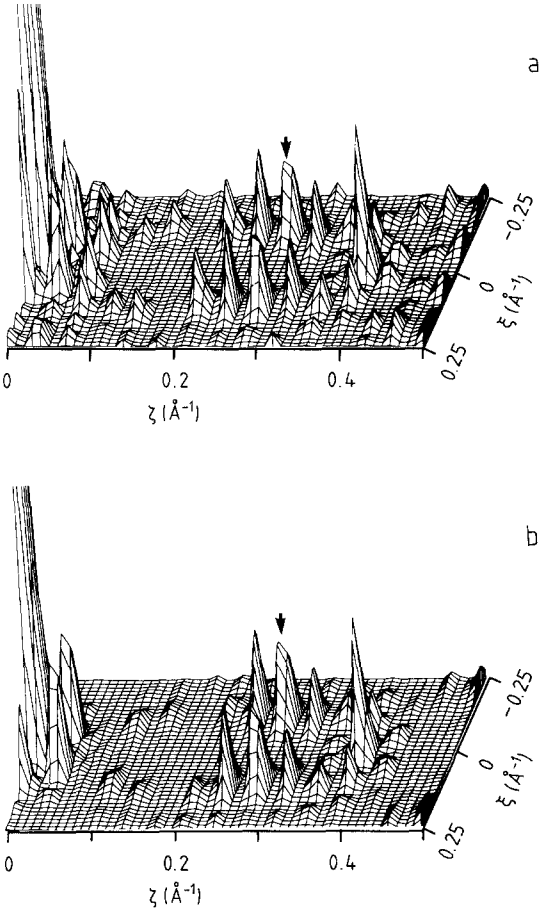

Fig. 13. a Squared modulus of the Fourier transform of the A-DNA atomic density (Arnott and Hukins 1972) decorated with the rather similar neutron scattering lengths for these atoms (0.665 (C), 0.94 (N), 0.58 (O), and 0.51 (P) in units of 10^{-12} cm). No hydrogen atoms have been added. The DNA density has been generated by application of the two-fold axis (C_{2x}) and 25 screw operations on the generating nucleotide residue which was averaged over the four bases. **b** Same as (**a**) without deoxyribose and phosphate parts. The *arrows* indicate the position of the 8th-layer peak

Formfactors of DNA

Figure 13 a shows the squared modulus of the molecular formfactor for a finite piece of A-DNA based on the optimised parameters of Arnott and Hukins (1972). The atomic positions are decorated with the neutron scattering lengths, the hydrogens are omitted and finite meridional correlation length is chosen. A realistic correlation length would cause a ζ-dependent decrease and increasing broadening of the layer peaks. These restrictions are, however, not relevant for the purpose of the present discussion.

The 8th-layer peak (indicated by arrow) is closest to h_w. No drastic change results in this region if the deoxyribose and phosphate parts are omitted (Fig. 13 b). The reason is demonstrated in Fig. 14. If one shrinks the bases to points at the center of their number density, Fig. 14 a is obtained. This is the folded X-type pattern for a discrete helix as discussed by Cochran et al. (1952). The average distance d of the base center from the helix axis ($d = 4.9$ Å for the A-conformation) serves as scaling factor for the ξ-dependence. If the number density of the bases is only coarsely represented by a Gaussian having the same first and second moments, Fig. 14 b is obtained. Since the bases are planar objects their formfactor is given by a line along their normals. They make an angle (tilt angle θ) of 20.3° with the helix direction. This formfactor suppresses all peaks of the point approximation (Fig. 14 a) which are too far off from the directions of the normals of the base planes. The intersection of both conditions is close to the 8th-layer peak which is located at $\xi \simeq 0.125$ Å^{-1}. The position of $\xi = (8/P_a) \tan\theta \simeq 0.105$ Å^{-1} would result from the base tilt. From the base center a value of $\xi \simeq 4.2/(2\pi d) \simeq 0.135$ Å^{-1} is obtained by using the location of the first maximum of the 3rd Bessel function.

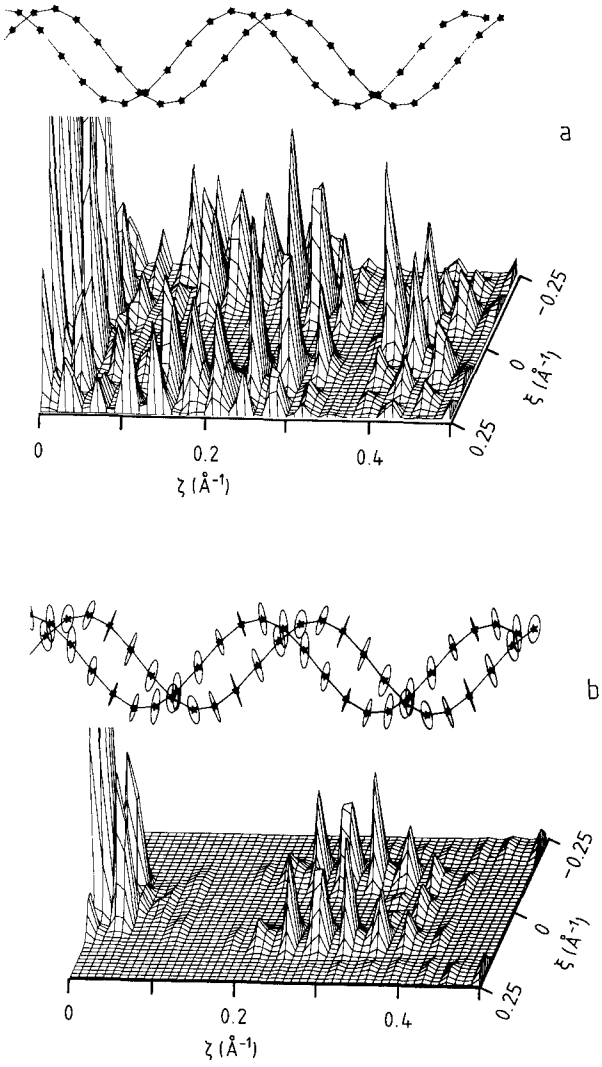

Fig. 14. **a** Same as Fig. 13 b but base centers, only. **b** The number density of the bases (Adenine, Thymine) is replaced by a Gaussian density with the same first and second moments. The shown ellipsoids of the real space density correspond to contours of constant density of the Gaussians. Using the average of the Gaussians over the four bases causes a vanishing of the small meridional 11th-layer peak

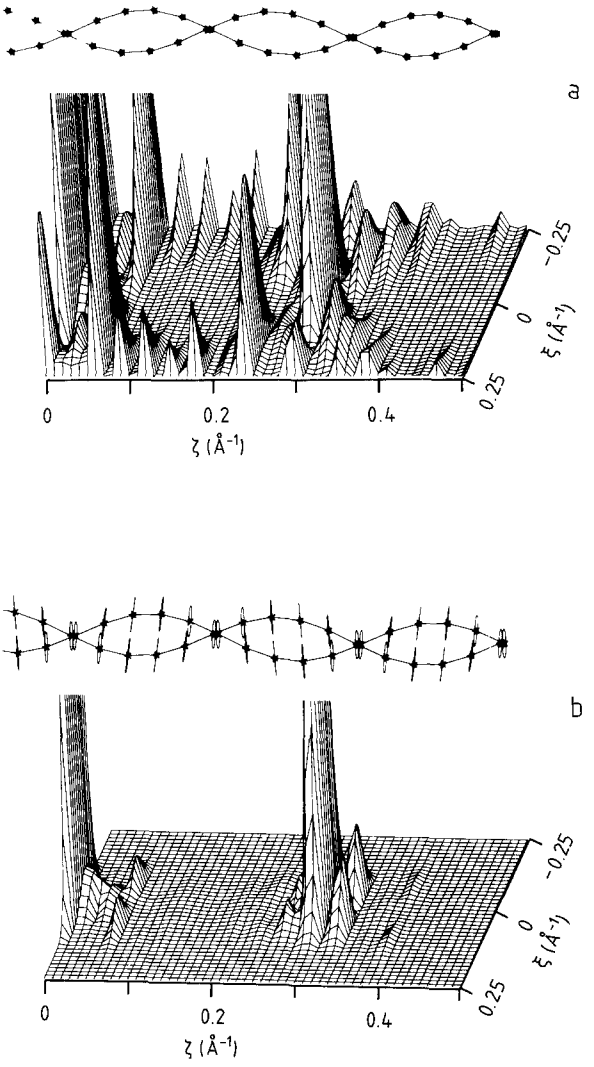

Fig. 15a and b. Same as Fig. 14 but for B-DNA, i.e. representation of the density of the bases by their centers (**a**) and by effective Gaussian densities (**b**), as indicated

One notes the qualitative similarity between the Gaussian approximation and Fig. 13 b. This similarity shows that e.g. the strong 6th-, 7th-, and 8th-layer peaks represent mainly two pieces of information, the distance d and the tilt θ of the bases from the helix axis. The small contribution of the other molecular groups can again be understood qualitatively by means of their formfactor. The normal of the sugar ring has no large component along the helix axis and the phosphate group is a globular object with a radius of $\simeq 1.5$ Å. Their formfactors do not therefore favour peaks at high layer lines both for A- and B-DNA. The analogous Gaussian approximation for the bases of the B-conformation is shown in Fig. 15. One notes in Fig. 15 a that the angle of the X-type pattern has opened up due the smaller value of $d \simeq 0.3$ Å for B-DNA. The smaller tilt of $\theta \simeq 6.3°$ favours the neighbourhood of the 10th layer, only. The C-conformation with $d \simeq 0.5$ Å and $\theta \simeq 8°$ (Arnott and Selsing 1975) is very similar to the B-form apart from the screw operation. This confirms the dominant contribution of the bases to the B- and C-peak (Langridge et al. 1960). The distance of the base planes d_p acts as a contraint on d, θ and the screw operation. It is determined to first order by the relation

$$d_p = p \cos\theta + d\alpha \sin\theta \qquad (2)$$

where $\alpha = 2\pi p/P$ denotes the screw angle. The values of $d_p = 3.37$, 3.38, and 3.33 Å result from the used parameters of A-, B-, and C-DNA, respectively.

Relation to experimental observations

The foregoing discussion might contribute to a better understanding of questions raised by the experimental observations. One question is the coexistence of A-, B-, and C-conformation in the NaDNA samples. Figure 13a confirms that the C-peak which was observed for samples No. 2 and No. 4 is not part of the A-conformation. This means that bases with small and large tilt angles coexist. The tilt angle distribution can be measured by the locally probing deuteron-NMR. An appreciable admixture of bases with small tilt angles (57%) has been identified for an A-DNA sample similar to our samples by means of this method which entails however a heat treatment for the labelling of the bases (Brandes et al. 1988).

The coexistence is metastable. Figure 9a shows that sample No. 4 contained a larger admixture of C-DNA than the equilibrated sample No. 2. Also, the very small admixture of B-DNA which was present for both samples was not recovered for sample No. 4 after the humidification period I. Metastability and coexistence seem to be the consequence of the different type of optimization for C-DNA as compared to A-, and B-DNA. For the C-conformation one observes the best overlap with the susceptibility of water but also a non-integer and ill-defined number of base pairs per turn. This favours one-dimensional correlation, only. The integer numbers of 11 and 10 base pairs per turn for the A-, and B-conformation support three-dimensional correlation as well. Large relaxation times are therefore plausible for C→A, B-transformations owing to the difference in the dimensionality of the correlation.

The close competition between these two types of optimization can also be recognized in the difference between Fig. 11a and c. As soon as the water influence becomes too strong (75% → 84% r.h.), the 10th-layer peak of B-DNA shifts to a somewhat higher value of ζ and the three-dimensional correlation vanishes – at least on the length scale of p_b. One-dimensional correlation causes a ζ-dependent broadening of the layer peaks. This is shown in Fig. 16 by the comparison of the meridional scans for the 10th- and 20th-layer peak. The deduced ratio in the FWHM of $\simeq 3.4$ may be compared to the value of 4 which would result for a free one-dimensional harmonic chain owing to the vanishing of the Debye-Waller factor (Mikeska 1973). The same ratio was observed for C-DNA (sample No. 1 at 75% r.h.).

The difference in the humidity dependence of the 8th-layer peak as compared to that of the 6th- and 7th-layer peak for A-DNA may be interpreted by a strong decrease of d and θ at the end of the humidification period I. As shown above, the 8th-layer peak represents the closest compromise between the formfactors due to d and θ. Therefore, one would expect a vanishing of the layer peaks in the sequence 6th, 7th, and 8th for the scan shown in Fig. 8b. This is in qualitative agreement with the observation for the 6th- and 7th-layer peak. On the other hand, one would expect indications of a decrease of the 8th-layer peak intensity, as well. Inspection of its profile (Fig. 9) shows that peak position *and* peak amplitude have not changed very much between the middle and the end of period I. We conclude therefore that the same is true for d and θ of the A-type bases of NaDNA.

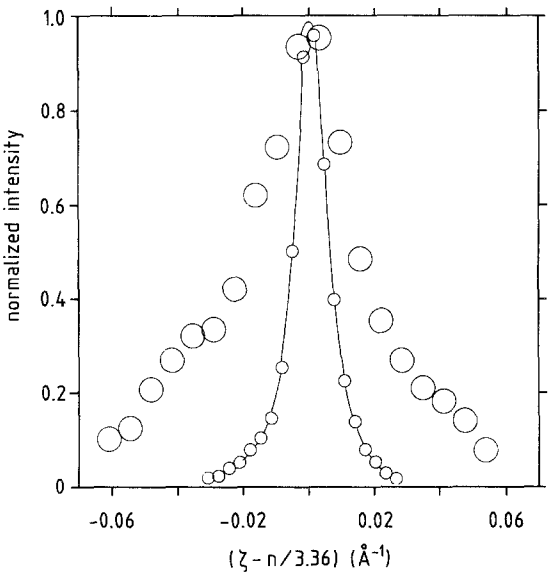

Fig. 16. B-DNA (sample No. 3, 84% r.h. D_2O): Comparison of two meridional scans through the 10th (*small circles*, $n=1$) and 20th layer (*large circles*, $n=2$). The peak intensities were normalized after the subtraction of the incoherent background

The comparison of the profiles shows, however, a reduction of the three-dimensional correlation. This is inherently connected with a decrease of the meridional correlation which causes a reduction of all three peaks, too. We observe indeed an increase of the width of the 8th-layer peak in meridional direction by $\simeq 36\%$ (39% after resolution correction) at the end of period I if we compare these two levels of humidity. A special water contribution of the 8th-layer peak in the humidity range above 75%, like e.g. an increasing bridging of the bases by water molecules, seems therefore not unlikely. Note that the modulus of this peak is both close to h_w *and* the inverse distance of neighbouring base planes.

Our limited experimental information about the H_2O/D_2O-contrast allows only for a compatibility consideration with the assumption that the main influence of water on the meridional correlation length is achieved by a direct and indirect bridging of the bases. The strong contrast of the C- and B-peak and the discussed dominant contribution of the bases in this

region of **h**-space would be compatible with the formation of a kind of dynamical precursor of a water spine similar to that observed for crystals of oligonucleotides (Kopka et al. 1983; Dickerson 1983). The specification as "dynamical precursor" takes into account that C-DNA and B-DNA humidified above 75% r.h. are rather close to the state of only one-dimensional correlation which implies inelasticity of the C- and B-peak (Mikeska 1973). The change in the shape of the C-peak on D_2O-hydration and the associated quasi-elastic spectra would indicate such a less rigid correlation between the assumed spine and the bases.

Acknowledgements. The initiation of this study would not have been possible without the encouragement and the collaboration of H. Stiller and U. Dahlborg. Measurements at Brookhaven National Laboratory benefitted from the stimulating cooperation with C. F. Majkrzak. The efficient technical help of K. Schönknecht in the measurements at Jülich was essential for their performance. One of us (H. G.) thanks the staff at Brookhaven National Laboratory, especially the Physics Department, for hospitality and assistance. Work at Brookhaven was supported by the Division of Material Sciences U.S. Department of Energy under Contract DE-AC02-76CH00016. One of us (A. R.) thanks the Swedish Medical Research Council for support. It is a pleasure to acknowledge all these efforts which rendered this work possible.

References

Arnott S, Hukins DWL (1972) Optimised parameters for A-DNA and B-DNA. Biochem Biophys Res Commun 47:1504–1509

Arnott S, Selsing E (1975) The conformation of C-DNA. J Mol Biol 98:265–269

Axe JD (1980) Fluctuations and freezing in a one-dimensional liquid: $Hg_{3-\delta}AsF_6$. In: Riste T (ed) Ordering in strongly fluctuating condensed matter systems. Plenum Press, New York, pp 399–414

Bacon GE (1975) Neutron diffraction. Clarendon Press, Oxford

Brandes R, Vold RR, Kearns DR, Rupprecht A (1988) A ^{2}H-NMR study of the A-DNA conformation in films of oriented Na-DNA: Evidence of a disordered B-DNA contribution. Biopolymers 27:1159–1170

Cochran W, Crick FHC, Vand V (1952) The structure of synthetic polypeptides. I. The transform of atoms on a helix. Acta Crystallogr 5:581–586

Cooper PJ, Hamilton LD (1966) The A-B conformational change in the sodium salt of DNA. J Mol Biol 16:562–563

Dahlborg U, Rupprecht A (1971) Hydration of DNA: A neutron scattering study of oriented NaDNA. Biopolymers 10: 849–863

Dahlborg U, Dimic V, Rupprecht A (1980) Study on the hydration of oriented DNA by the neutron scattering technique. Phys Scr 22:179–187

Demarco C, Lindsay SM, Pokorny M, Powell J, Rupprecht A (1985) Interhelical effects on the low-frequency modes and phase transitions of Li- and Na-DNA. Biopolymers 24:2035–2040

Dickerson RE (1983) The DNA helix and how it is read. Sci Am 249:86–103

Edwards GS, Genzel L, Peticolas WL, Rupprecht A (1986) Measurements of a large anisotropy in the swelling of oriented DNA films in aqueous solution. Biopolymers 25:223–227

Falk M, Hartmann KA Jr, Lord RC (1962) Hydration of deoxyribonucleic acid. I. A gravimetric study. J Am Chem Soc 84:3843–3846

Falk M, Hartmann KA Jr, Lord RC (1963) Hydration of deoxyribonucleic acid. II. An infrared study. J Am Chem Soc 85:387–394

Franklin RE, Gosling RG (1953) The structure of sodium thymonucleate fibers. II. The cylindrically symmetrical Patterson function. Acta Crystallogr 6:678–685

Franks F (1972) Water – A comprehensive treatise. The physics and physical chemistry of water, vol. 1. Plenum Press, New York London, p 349

Fuller W, Wilkins MHF, Wilson HR, Hamilton LD (1965) The molecular configuration of deoxyribonucleic acid. IV. X-ray diffraction study of the A form. J Mol Biol 12:60–80

Fuller W, Forsyth VT, Mahendrasingam A, Pigram WJ, Greenall RJ, Langan P, Bellamy K, Al-Hayalee Y, Mason SA (1989) The location of water around the DNA double-helix. Physica B156 & 157:468–470

Grimm H, Stiller H, Majkrzak CF, Rupprecht A, Dahlborg U (1987) Observation of acoustic umklapp phonons in water-stabilized DNA by neutron scattering. Phys Rev Lett 59:1780–1783

Grimm H, Stiller H, Majkrzak CF, Rupprecht A (1989) Neutron scattering study of the hydration hull of DNA by H_2O/D_2O-exchange. Physica B156 & 157:464–467

Kopka ML, Fratini AV, Drew HR, Dickerson RE (1983) Ordered water structure around a B-DNA dodecamer. A quantitative study. J Mol Biol 163:129–146

Langridge R, Marvin DA, Seeds WE, Wilson HR, Hooper CW, Wilkins MHF, Hamilton LD (1960) The molecular configuration of deoxyribonucleic acid. II. Molecular models and their Fourier transforms. J Mol Biol 2:38–64

Marvin DA, Spencer M, Wilkins MHF, Hamilton LD (1961) The molecular configuration of deoxyribonucleic acid. III. X-ray diffraction study of the C-form of the lithium salt. J Mol Biol 3:547–565

Mikeska HJ (1973) Phonon peaks in the dynamic structure factor of lattices without long range order. Solid State Commun 13:73–76

Rupprecht A (1966) Preparation of oriented DNA by wet spinning. Acta Chem Scand 20:494–504

Saenger W, Hunter WN, Kennard O (1986) DNA conformation is determined by economics in the hydration of phosphate groups. Nature 324:385–388

Schreiner LJ, Pintar MM, Dianoux AJ, Volino F, Rupprecht A (1988) Hydration of NaDNA by neutron quasi-elastic scattering. Biophys J 53:119–122

Vineyard GH (1954) Multiple scattering of neutrons. Phys Rev 96:93–98